A&A manuscript no.
(will be inserted by hand later)

Your thesaurus codes are:
06 (08.01.3; 08.05.1; 08.13.2; 08.23.2)

ASTRONOMY
AND
ASTROPHYSICS
22.8.1996

Stationary hydrodynamic models of Wolf-Rayet stars with optically thick winds

A. Heger and N. Langer

Max-Planck-Institut für Astrophysik, Karl-Schwarzschild-Str. 1, Postfach 1523, D-85740 Garching b. München, Germany

Received , accepted

Abstract. We investigate the influence of a grey, optically thick wind on the surface and internal structure of Wolf-Rayet (WR) stars. We calculate hydrodynamic models of chemically homogeneous helium stars with stationary outflows, solving the full set of stellar structure equations from the stellar center up to well beyond the sonic point of the wind, including the line force originating from absorption lines in a parameterized way. For specific assumptions about mass loss rate and wind opacity above our outer boundary, we find that the iron opacity peak may lead to local super-Eddington luminosities at the sonic point.

By varying the stellar wind parameters over the whole physically plausible range, we show that the radius of the sonic point of the wind flow is always very close to the hydrostatic stellar radius obtained in WR star models which ignore the wind. However, our models confirm the possibility of large values for observable WR radii and correspondingly small effective temperatures found in earlier models.

We show further that the energy which is contained in a typical WR wind can not be neglected. The stellar luminosity may be reduced by several 10 %, which has a pronounced effect on the mass-luminosity relation. I. e., the WR masses derived for a given luminosity may be considerably larger. Thereby, also the momentum problem of WR winds is considerably reduced, as well as the scatter in the $\dot{M}$ vs. M diagram for observed hydrogen-free WN stars.

Key words: Wolf-Rayet stars – mass loss – massive stars

1. Introduction

Wolf-Rayet (WR) stars are thought to represent a late evolutionary stage of stars initially more massive than $25\ \mathrm{M}_\odot - 40\ \mathrm{M}_\odot$, which occurs as a result of the loss of all or at least the major part of their hydrogen-rich envelope (e. g. Chiosi & Maeder 1986, Lamers et al. 1991, Maeder & Conti 1994).

Although WR stars are among the most luminous stellar objects in the sky and contribute substantially to the chemical and dynamical evolution of galaxies, even their basic properties, e. g. their radii or their luminosities, are still not well known today (Morris 1995, Moffat & Marchenko 1996). This arises mainly from the fact that WR stars are obscured by their own dense stellar wind, the origin of which is not yet understood and which renders the modeling of WR stars and their atmospheres difficult (Hamann 1995, Hillier 1995, Schmutz 1995a, Owocki & Gayley 1995).

WR atmosphere and wind calculations usually use an inner boundary condition at a radius R_h, below which the star is assumed to be essentially hydrostatic. The values used for R_h in recent WR wind models (Lucy & Abbott 1993; Springmann 1994; Schmutz 1995b) and WR atmosphere models (cf. Hamann et al. 1995) are mostly factors of several larger than those radii which are predicted by hydrostatic stellar structure and stellar evolution calculations (Maeder & Meynet 1987, Langer 1989a).

This ambiguity concerning the "hydrostatic radii" of WR stars – which we want to define here as the radius of the sonic point in the outflow – is persisting because the sonic point is in many cases not located in the observable, optically thin part of the wind (cf. Schaerer 1996), but on the other hand it is also not included in standard hydrostatic stellar model calculations. Note that our purely kinematic definition of the hydrostatic radius is not affected by the wavelength dependence of the optical depth which concerns, e. g., any definition of the photospheric radius.

In the present paper we present hydrodynamic stellar models with an outer boundary condition which is located in the supersonic part of the wind flow and allows thus, when appropriate outer boundary conditions are provided, a self-consistent determination of the physi-

Send offprint requests to: A. Heger

cal conditions at the hydrostatic radius, including the radius itself. Furthermore, since – according to the theory of radiation driven winds of hot stars (Kudritzki 1988) – the stellar mass loss rate is fixed in the vicinity of the sonic point, we hope that, by specifying also the thermodynamic conditions in this part of the wind flow, our models can yield clues and constraints for theories of the origin of the intense WR winds.

These strong winds may also have an important influence on the luminosities of WR stars, since the energy required to drive the wind, i. e. the potential energy which the wind matter has to overcome and the kinetic and thermal energy carried away by the wind, may not be negligible. We are able to investigate this effect quantitatively with our method, since it includes the equations of energy conservation and transport.

This paper is organized as follows. In Section 2 we present the computational methods and physical assumptions used. In Section 3, we investigate the vicinity of the sonic point of a 15 $M_\odot$ helium star and discuss the influence of different mass loss rates on the stellar structure. The radial decline of the photon luminosity due to mass loss is elaborated in Section 4, and incorporated in a mass-luminosity relation for "standard" wind parameters in Section 5 where we compare our results with observational data. Our conclusions are summarized in Section 6.

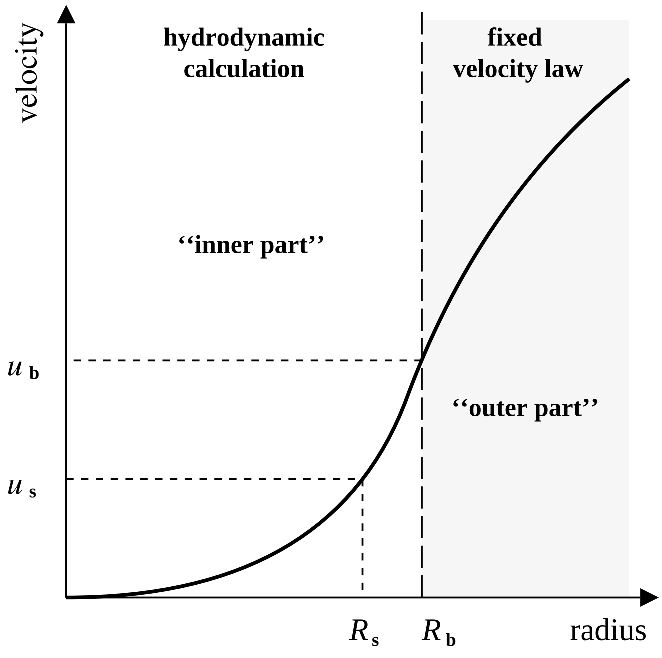

Fig. 1. "Inner" and "outer" part of the model. The border line at $R_{\rm b}$ is defined by a given boundary velocity $u_{\rm b}$, the sonic point radius $R_{\rm s}$ by the condition that the velocity is equal to the local sound velocity $c_{\rm s}$ (cf. Eq. (18)). This velocity is denoted as $u_{\rm s}$. $u_{\rm b}$ is chosen such that the sonic point is located at a radius $R_{\rm b} > R_{\rm s}$

2. Computational methods and physical models

In our numerical scheme, we divide the star into two regions (see Fig. 1), which we designate in the following as

– the **inner** part, where we solve the full set of hydrodynamic stellar structure equations, and
– the **outer** part, for which we prescribe a fixed radial dependence of the wind velocity and which yields the outer boundary conditions for the inner part.

The boundary between inner and outer part is fixed by the choice of a boundary velocity $u_{\rm b}$. In most cases, we adopt $u_{\rm b} = 10^7$ cm s^{-1}, which corresponds to several times the sonic point velocity $u_{\rm s}$ and guarantees the sonic point to be located in the inner part of our models. On the other hand, this value of $u_{\rm b}$ is sufficiently small to yield an optical depth well above one at the outer boundary of the inner part of our models (cf. e. g. Table 1 in Section 3.3), which allows the use of the diffusion approximation for the radiative energy transport. We found the physical conditions at the sonic point to be insensitive to the exact choice of $u_{\rm b}$.

2.1. Outer part

In the outer part, we assume a stationary outflowing grey wind which obeys a given velocity law $u\,(r)$. The mass M of the star and the mass loss rate $\dot{M}$ can be assumed to be constant in this region (cf. Section 2.3). Following Springmann (1994), we use a generalized velocity law as

$$u\,(r) = u_{\rm b} + (u_\infty - u_{\rm b}) \left(\beta_1 x + (1-\beta_1)\, x^{\beta_2}\right)^{\frac{1}{2}} \tag{1}$$

with

$$x := 1 - \frac{R_{\rm b}}{r} \quad , \quad \beta_1 = 0.35 \quad , \quad \beta_2 = 8 \quad . \tag{2}$$

This choice of β_1 and β_2 is not completely free of arbitrariness; however, a variation of these parameters in the range discussed by Springmann (1994) would not alter any of our conclusions. The terminal velocity of the wind is denoted as u_∞ and we adopt

$$u_\infty = \sqrt{\frac{2GM}{R_{\rm s}}} \tag{3}$$

which yields values in the observed range (cf. Hamann et al. 1995).

For comparison, a simple velocity law of the form

$$u\,(r) = u_{\rm b} + (u_\infty - u_{\rm b})\, x^\beta \tag{4}$$

with $\beta = 1$ corresponds to a weaker acceleration close to the sonic point, whereas the the acceleration is stronger at lager radii. A given mass loss rate $\dot{M}$ (for convenience we define $\dot{M} := -\frac{\mathrm{d}M}{\mathrm{d}t}$) then allows to determine the density structure in the wind as

$$\rho(r) = \frac{\dot{M}}{4\pi r^2 u(r)} \quad . \tag{5}$$

Together with the *effective opacity*

$$\kappa_{\mathrm{eff}} := \frac{4\pi r^2 c}{L}\left(u\frac{\mathrm{d}u}{\mathrm{d}r} + \frac{GM}{r^2}\right) \tag{6}$$

(Lucy & Abbott 1993), which is the opacity required to drive the wind according to the assumed velocity law $u(r)$, the temperature stratification of the spherically extended grey atmosphere, i. e. the outer part of our model, is given by (Lucy 1971, 1976):

$$T(r) = T_{\mathrm{p}}\sqrt[4]{W + \frac{3}{4}\tilde{\tau}} \tag{7}$$

where

$$W := \frac{1}{2}\left(1 - \sqrt{1 - \left(\frac{R_{\mathrm{p}}}{r}\right)^2}\right) \tag{8}$$

is the dilution factor of the radiation and

$$\tilde{\tau}(r) := \int_r^\infty \kappa\rho\left(\frac{R_{\mathrm{p}}}{r}\right)^2 \,\mathrm{d}r \tag{9}$$

is the *effective optical depth.* It differs from the usual definition of an optical depth τ by the geometric factor $(R_{\mathrm{p}}/r)^2$. In these formulae, c denotes the velocity of light, G the gravitational constant and L the local radiative luminosity. The photospheric radius R_{p} is defined by

$$\tilde{\tau}(R_{\mathrm{p}}) \stackrel{!}{=} \frac{2}{3} \quad . \tag{10}$$

According to Lucy & Abbott (1993) we adopt $W = \frac{1}{2}$ for $\tilde{\tau} > \frac{2}{3}$. The photospheric temperature T_{p}, which is the effective temperature of the star, can then be calculated from the stellar photon luminosity by

$$T_{\mathrm{p}} = \sqrt[4]{\frac{L}{4\pi\sigma {R_{\mathrm{p}}}^2}} \quad , \tag{11}$$

where σ is the Stefan-Boltzmann constant.

The main purpose of the calculation of the outer part of our model is to provide a temperature at the radius R_{b} as outer boundary condition for the inner part. However, though this could have been more easily achieved by adopting the temperature at R_{b} as a free parameter, it allows also a realistic estimate of the photospheric conditions, i. e. a photospheric temperature and radius, though these values must remain somewhat uncertain, mainly due to our restriction to a grey atmosphere model.

2.2. Inner part

In the inner part we solve the Lagrangian hydrodynamic stellar structure equations (see e. g. Kippenhahn & Weigert 1991) with the implicit Henyey-method (Henyey et al. 1964, Hofmeister et al. 1964). For the addition of a mass source term to obtain stationary models see Section 2.3.

For $T < 10^8$ K we use the OPAL opacity tables from Iglesias et al. (1992), and Los Alamos tables (Huebner et al. 1977) for higher temperatures. Convection is treated according to the standard mixing length theory, with a mixing length parameter of $\alpha_{\mathrm{MLT}} = 2$. The outer boundary condition as described above guarantees that the optical depth τ is larger than $\frac{2}{3}$ at the outermost grid point and therefore in the whole inner part of our model.

In order to obtain a realistic estimate of the total force acting on the outflowing material, we included the so called line force as additional term into the momentum equation. According to Springmann (1994), the acceleration due to the line force can be written as

$$g_{\mathrm{lines}} = n_{\mathrm{L}}\frac{L}{\dot{M}cu_\infty}u\frac{\mathrm{d}u}{\mathrm{d}r}\mathcal{F} \quad , \tag{12}$$

where n_{L} is the number of optically thick lines per frequency interval $\nu \ldots \nu\left(1 + \frac{u_\infty}{c}\right)$. The value of n_{L} can not be determined precisely at present and has therefore to be treated as a free parameter in our model, with realistic values being of the order of $n_{\mathrm{L}} = 20 \ldots 40$ (cf. Springmann 1994). The factor

$$\mathcal{F} := \left\langle\frac{\mathrm{d}u_{\mathrm{l}}}{\mathrm{d}l}\right\rangle \Big/ \frac{\mathrm{d}u}{\mathrm{d}r} \quad , \tag{13}$$

where l is the line element of the radiation propagation and $\langle\cdot\rangle$ denotes the mean over all directions (see Springmann 1994), depends on geometric details and is of the order of one in the vicinity of the sonic point and below ($\mathcal{F} \approx 0.6$). We use equation (56) of Springmann (1994) to evaluate $\mathcal{F}$.

2.3. Stationarity

In order to obtain well defined, and therefore well comparable WR star models, we calculate stationary models. For that, we introduce a mass source into the models which exactly balances the mass loss. We choose a mass source which is distributed over the whole star, being proportional to the local density ρ. This induces a mass flow through each shell with radius r which is proportional to the total mass below this radius, i. e. $\dot{m}(r) \sim m(r)$, where m is the mass coordinate and $\dot{m}$ the mass loss rate as a function of r. Due to the fact that the region of our models where non-zero velocities affect their structure, i. e. the outermost part of the star, contains only a negligible part of the total stellar mass (typically 10^{-9} of the total stellar mass are contained in the layers between the sonic point and the photosphere), the mass source term is certainly negligible there.

Further inwards, the mass source term does not affect the structure because it is governed by thermal and hydrostatic equilibrium, a situation which remains valid also in a mass losing WR star since the mass loss time-scale

$$\tau_{\dot{\mathrm{M}}} := \frac{M}{\dot{M}} \tag{14}$$

is longer than the thermal time-scale

$$\tau_{\mathrm{KH}} := \frac{GM^2}{2RL} \quad , \tag{15}$$

and certainly also longer than the dynamical time scale. E. g., for our 15 $\mathrm{M}_\odot$ standard model (see below) we find $\tau_{\mathrm{KH}} \approx 10^4$ yr whereas $\tau_{\dot{\mathrm{M}}} \approx 3\,10^5$ yr.

The nuclear time scale of this model, which is about $\tau_{\mathrm{nuc}} \approx 4.4\,10^5$ yr, is even longer than the mass loss time-scale. Therefore our neglect of changes of the chemical composition due to nuclear burning is certainly justified. Finally, it has been shown by Langer (1989a) that chemical gradients in the interior of hydrogen-free WR stars have practically no effect on the whole thermal and mechanical structure of the star. For this reason, despite our assumption of chemical homogeneity, the results obtained in the present work also hold for such stars which have obtained significant abundances of carbon and oxygen in the interior due to core helium burning.

For test purpose, we have compared our stationary models with models including all time dependent terms but without a mass source term, computed by applying a realistic mass loss and changes in the chemical profiles just as in standard stellar evolution calculations. A comparison of these evolutionary models with our stationary models at exactly the same stellar mass confirmed that all relevant quantities are practically identical. As an example, for a 15 $\mathrm{M}_\odot$ model we find, that the luminosity of the evolutionary model L_{ev} and the luminosity of our stationary model L_{stat} differ only by

$$\left| \frac{L_{\mathrm{ev}} - L_{\mathrm{stat}}}{L_{\mathrm{ev}}} \right| \lesssim 4\,10^{-3} \quad .$$

2.4. Standard parameters

We use the mass dependent power law mass loss formula

$$\dot{M} = K \left(\frac{M}{\mathrm{M}_\odot} \right)^{\alpha} \tag{16}$$

derived by Langer (1989b), adopting $K = 5\,10^{-8}\ \mathrm{M}_\odot\ \mathrm{yr}^{-1}$ and $\alpha = 2.6$. We denote the mass dependent mass loss rate using these special parameters our *standard mass loss rate* $\dot{M}_0$.

Most of our calculations were performed using a 15 $\mathrm{M}_\odot$ helium star model. Its chemical composition is that of a massive helium core resulting from central hydrogen burning, assuming solar metallicity. Therefore our model includes no hydrogen and 98 % ^{4}He, 1.5 % ^{14}N and 0.5 % other elements, by mass. Furthermore, for the reasons outlined above the model is assumed to be chemically homogeneous. According to Springmann (1994), for the line density we adopt $n_{\mathrm{L}} = 37$. In the outer part we use the effective opacity κ_{eff} (cf. Eq. (6)) which is consistent with the adopted velocity law (Eq. (1)). We do not consider companion stars, magnetic fields or rotation. This model will be called our *standard model* and it is characterized by the following typical values:

It has a convective core mass of $M_{\mathrm{c}} \approx 11\ \mathrm{M}_\odot$, a standard mass loss rate of $\dot{M}_0(15\ \mathrm{M}_\odot) = 5.71\,10^{-5}\ \mathrm{M}_\odot\ \mathrm{yr}^{-1}$, a sonic point radius of $R_{\mathrm{s}} = 1.1\ \mathrm{R}_\odot$ and a sonic point temperature of $T_{\mathrm{s}} = 2.54\,10^5$ K. The optical depth at the sonic point is $\tau_{\mathrm{s}} = 52.9$. The photospheric radius of the standard model is $R_{\mathrm{p}} = 37.9\ \mathrm{R}_\odot$ and the temperature at the photosphere is $T_{\mathrm{p}} = 2.06\,10^4$ K. For the terminal wind velocity we get a value of $u_\infty = 2.26\,10^3\ \mathrm{km\ s}^{-1}$.

This model has a total rate of nuclear energy production L_{nuc} of $10^{5.4}\ \mathrm{L}_\odot$, where the "nuclear luminosity" L_{nuc} is defined as

$$L_{\mathrm{nuc}} = \int_0^M \epsilon_{\mathrm{nuc}}\, \mathrm{d}m \quad , \tag{17}$$

with ϵ_{nuc} being the local rate of nuclear energy generation.

3. The Structure of the outer layers

3.1. Effects of the wind line force parameter

Here, we investigate the influence of the stellar wind properties on the structure of the layers in the vicinity of the sonic point. First we calculate models with different values of the line force parameter n_{L} for a fixed mass loss rate, with the wind velocity law (1) and the effective opacity κ_{eff} according to (6). Fig. 2 shows the resulting velocity profiles for three different values of n_{L}, together with the radial dependence of the isothermal sound velocity

$$c_{\mathrm{s}} = \sqrt{\Re T/\mu} \quad , \tag{18}$$

which is practically the same for all three models. Fig. 2 shows that the line force parameter n_{L} has almost no influence on the sonic point radius R_{s}. Note that larger values of n_{L} than about 50 are from the physical point of view not sensible, because for $c_{\mathrm{s}} n_{\mathrm{L}} \gtrsim u_\infty$ the lines start to overlap.

Our models allow for the first time, to evaluate quantitatively the often applied approximation that the hydrostatic stellar radius is equal to R_{s}. For subsonic velocities, i. e. $r < R_{\mathrm{s}}$, the matter becomes very soon hydrostatic. If we define a hydrostatic radius R_{h} such that the inertia of the matter is negligible compared to the gravitational acceleration, i. e. less than 1 %, we find that it is generally only of the order of 0.01 $\mathrm{R}_\odot$ smaller than the sonic point radius, depending slightly on the wind parameters.

For the standard model we find $R_{\rm s} - R_{\rm h} = 3.2\,10^{-3}\ {\rm R}_\odot$. Fig. 2 shows, that also the line force parameter does not affect the velocity structure below $R_{\rm h}$, and only the supersonic part of the velocity stratification does significantly change for different values of $n_{\rm L}$.

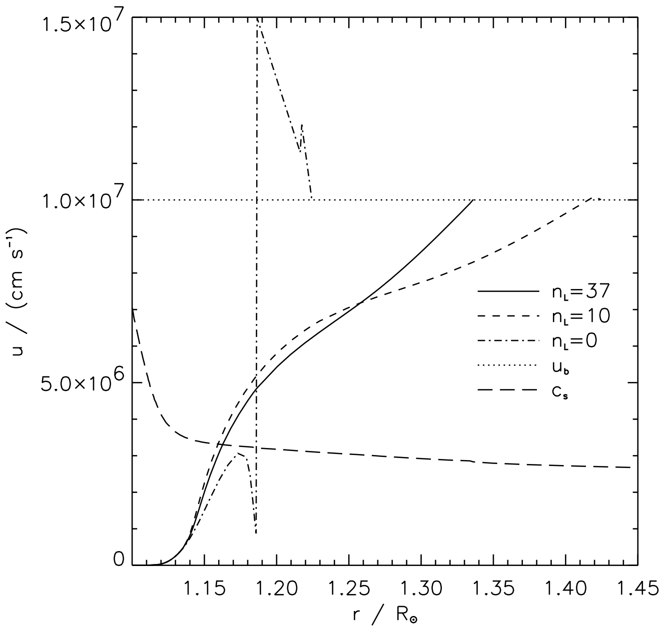

Fig. 2. Velocity stratification in the vicinity of the sonic point for different values of $n_{\rm L}$ for a 15 ${\rm M}_\odot$ helium star. The transition velocity $u_{\rm b} = 10^7$ cm s^{-1} and the isothermal sound velocity $c_{\rm s}$ are also shown. In the outer part the velocity law (1) with effective opacity (6) is used, but not shown in this figure. The mass loss rate of the models is $\dot{M} = 0.1\,\dot{M}_0$.

The model without line force contains a series of convection zones close to the sonic point, resulting in density and velocity inversions. Since the velocity profile shows unresolved jumps, we do not believe that this is physically realized. In contrast, the models including the line force vary smoothly from the subsonic to the supersonic region of the wind. A major difference between the velocity structures of the two models with $n_{\rm L} \neq 0$ is only found in the supersonic region. In the subsonic region, the velocity structure becomes independent of the line force parameter.

3.2. The Eddington-factor

To investigate the force balance in the vicinity of the sonic point, we define

$$\Gamma(r) := \frac{L(r)}{L_{\rm Ed}(r)} = \frac{\kappa L(r)}{4\pi c G m(r)} \quad , \tag{19}$$

which is the local photon luminosity L in units of the local Eddington luminosity $L_{\rm Ed}$. Here we use a definition which takes into account the total opacity κ instead, as sometimes used, only the electron scattering opacity $\kappa_{\rm es}$. Γ has an important influence on the mass loss rate of the star, since $\Gamma = 1$ means that the gravitational force is balanced by the radiation pressure gradient.

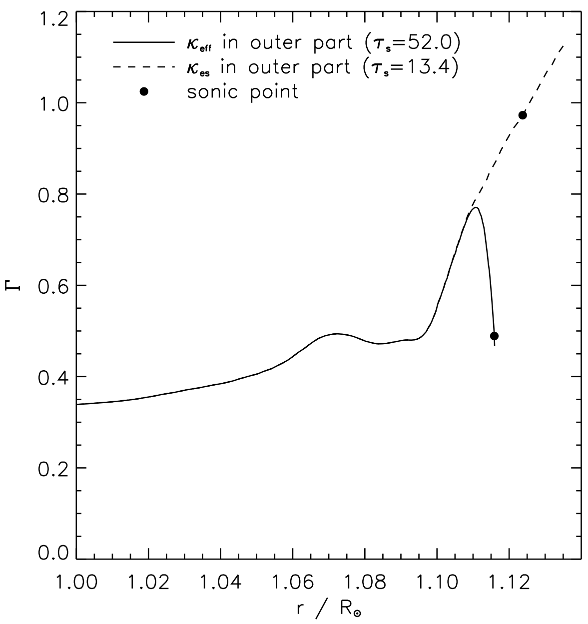

Fig. 3. Γ (see Eq. (19)) as function of the radius for two different opacities used in the outer part of the model, and using $n_{\rm L} = 10$ in the inner part. The solid line shows the standard model, where the effective opacity $\kappa_{\rm eff}$ according to (6) is used, whereas the dashed line shows a model where only the Thompson scattering opacity $\kappa_{\rm es}$ is taken into account for $u > u_{\rm b}$. In the second case, local super-Eddington luminosities are obtained. For both models, the sonic point is marked by a dot.

Since the inner and outer part of the model do only interact via the boundary conditions at the transition point, the details of the velocity law and the wind structure in the outer part are not relevant for the inner part of the model. For a given boundary velocity $u_{\rm b}$, only the temperature at the transition point is important. Fig. 3 compares two models with different assumptions on the opacity in the outer part. The first model (solid line) is our standard model, using the effective opacity $\kappa_{\rm eff}$ (cf. Eq. (6)), whereas for the second model (dashed line) only the Thompson scattering opacity $\kappa_{\rm es}$ is taken into account, leading to an optically less thick atmosphere and therefore to lower temperatures in the vicinity of the sonic point ($T_{\rm s} = 2.02\,10^5$ K, in contrast to $T_{\rm s} = 2.55\,10^5$ K in the standard model). In the model with lower sonic point temperature, the iron opacity peak (Iglesias et al. 1992) is located very close to the sonic point, leading to super-Eddington luminosities in its vicinity (cf. Fig. 3).

The fact that, for certain wind parameters, the shift of the iron opacity peak to the vicinity of the sonic point of the wind flow can result in a local super-Eddington luminosity at the sonic point, may have implications for the understanding of the observed very high Wolf-Rayet mass loss rates, since, according to the theory of stellar winds, the mass loss rate is basically fixed by the physical conditions at the sonic point. However, to explain not a single object but at least a class of WR stars, requires a self-regulating mechanism which establishes the wind stratification such that the location of the opacity peak coincides with the sonic point. Despite convection can strongly reduce the effective Eddington luminosity for a subsonic location of the opacity peak (Schaerer 1996), this appears not possible if it is located at the sonic point or beyond.

Whether or not such a self-regulation can be obtained must be left to future studies. However we want to point out at least one possible scenario which might work in this way. Glatzel et al. (1993) have found that hydrostatic helium star models, i. e. models which ignore the effect of a strong dense outflow, are unstable to the so called "strange mode" pulsations, for masses above $\approx 4\ M_\odot$. This instability is extremely violent, i. e. its growth time is the dynamical time-scale of the star, i. e. roughly the pulsation time-scale itself. Therefore, a quiescent hydrostatic surface structure is inhibited for these stars according to the results of Glatzel et al. (1993).

We propose the possibility that the strange mode pulsations may act as an initiator of the strong WR wind, by lifting the surface material to a certain level and pushing it to appreciable velocities – it is to be noted, that the ability of the strange mode pulsations to do this has been shown by the non-linear hydrodynamic calculations of Kiriakidis (1993) – thus considerably increasing the density at and well beyond the sonic point of the flow. Within this scenario, it would still be left to the radiation field to accelerate the material to the very large velocities observed in WR winds (cf. e. g. Hamann et al. 1995), and though we have no tool to demonstrate that this is actually possible we may refer to the work of Lucy & Abbot (1993), which showed that the radiation field of WR stars may be able to transform several times the total photon momentum to the wind flow. In any case the star has not the possibility to let the matter initially accelerated by the pulsations fall back and settle on the stellar surface, because the hydrostatic state is so unstable.

The lack of observational evidence of WR pulsations with appropriate periods (Glatzel et al. 1993) can not be considered as a counterargument of our hypothesis, since the nonlinear behavior of the strange mode pulsations, and especially their coupling with the radiation pressure force due to absorption lines need still to be explored.

In a recent paper, Eichler et al. (1995) proposed a feedback between surface temperature and mass loss rate of WR stars. Higher mass loss rates would cause the wind to become more optically thick and therefore yield higher surface temperatures and lower opacities which would then decrease the mass loss rate again. Lower mass loss rates should analogously give the vice versa effect. Our results presented above indicate that such a mechanism may in fact work in WR atmospheres.

3.3. Effects of different mass loss rates

Here, we study models with different mass loss rates in the range of $0.03\ldots20$ times the standard mass loss rate $\dot{M}_0$, calculating 46 different models in total. Apart from that we use the standard parameters (see Section 2.4).

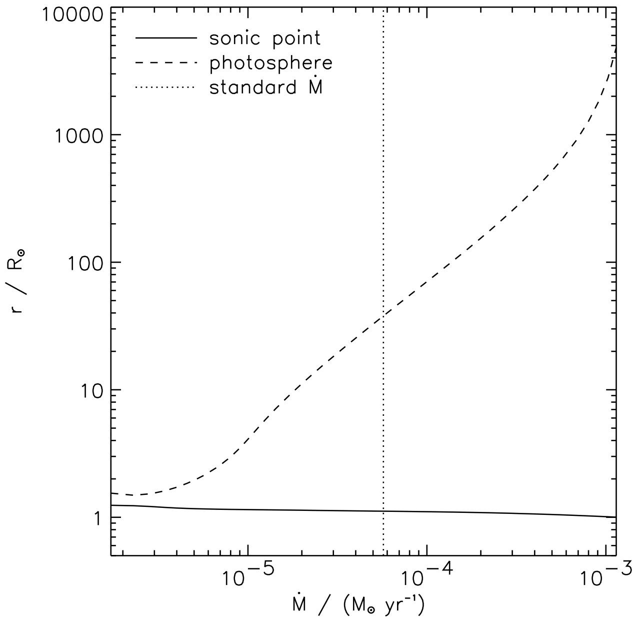

Fig. 4. Photospheric radius (dashed line) and sonic point radius (solid line) as function of the mass loss rate $\dot{M}$. The dotted line marks the standard mass loss rate $\dot{M}_0$. For the opacity and the line force we used our standard parameters (cf. Section 2.4).

Higher densities in the wind lead to larger optical depths (cf. Table 1) and higher temperatures at the sonic point. As shown in Section 3.2, this has a major influence on the opacity in that region. The sonic point itself shifts to higher velocities, because the velocity of sound c_s is proportional to $\sqrt{T}$ (cf. Eq. 18). In the mass loss rate range of $\dot{M} = 0.2\,\dot{M}_0\ldots5\,\dot{M}_0$ we observe that the luminosity at the sonic point decreases by about 4 % (cf. Fig. 7 below). This may explain the slight shrinking of the sonic point radius (see Fig. 4).

With increasing mass loss rate $\dot{M}$ the density ρ in the wind is increasing. Assuming that the opacity in the outer part of the model remains at least constant, the optical thickness of the wind rises. Obviously the photospheric

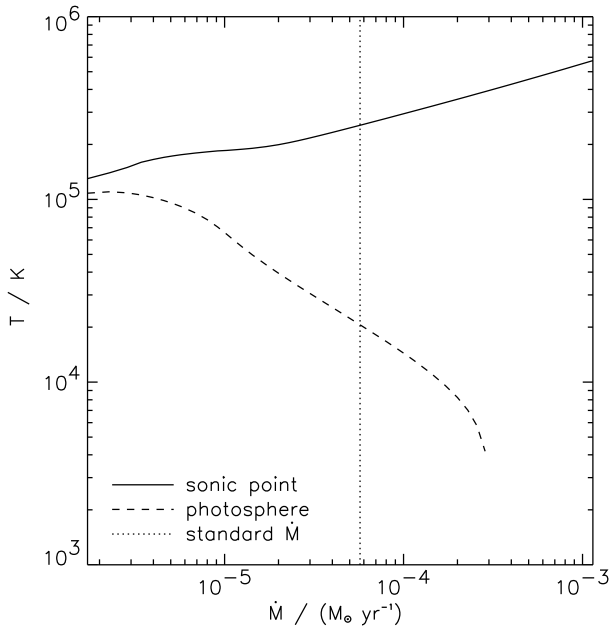

Fig. 5. Sonic point temperature (solid line) and effective temperature (dashed line) as function of the mass loss rate $\dot{M}$. The dotted line marks the standard mass loss rate $\dot{M}_0$. For the opacity and the line force we used our standard parameters (cf. Section 2.4).

radius $R_{\rm p}$ (cf. Fig. 4) becomes larger and the photospheric temperatures $T_{\rm p}$ (cf. Fig. 5) smaller.

Central density $\rho_{\rm c}$ and central temperature $T_{\rm c}$ change only very little for different mass loss rates, as can be seen in Table 1. Accordingly, the nuclear luminosity $L_{\rm nuc}$ increases only very little with rising mass loss rate $\dot{M}$. In the vicinity of $\dot{M}_0$ we find

$$\frac{\mathrm{d}\ln(L_{\rm nuc})}{\mathrm{d}\ln(\dot{M})} \approx -3.54\,10^{-3} \quad .$$

Table 1. Nuclear luminosity $L_{\rm nuc}$ (cf. Eq. (17)), central density $\rho_{\rm c}$, central temperature $T_{\rm c}$, convective core mass $M_{\rm c}$, and optical depth at the sonic point $\tau_{\rm s}$, for a 15 $\mathrm{M}_\odot$ helium star for several values of the mass loss rate $\dot{M}$ in units of the standard mass loss rate $\dot{M}_0$.

$\frac{\dot{M}}{\dot{M}_0}$	$\log\left(\frac{L_{\rm nuc}}{\mathrm{L}_\odot}\right)$	$\log\left(\frac{\rho_{\rm c}}{\mathrm{g\ cm^{-3}}}\right)$	$\log\left(\frac{T_{\rm c}}{\mathrm{K}}\right)$	$\frac{M_{\rm c}}{\mathrm{M}_\odot}$	$\tau_{\rm s}$
0.2	5.4676	2.634451	8.28486	10.7	12.8
0.5	5.4681	2.634443	8.28488	10.7	26.0
1.0	5.4688	2.634432	8.28491	10.8	52.9
2.0	5.4702	2.634416	8.28497	10.8	111.0
5.0	5.4738	2.634376	8.28512	11.0	325.1

Also, the size of the convective core increases only by about 3 % for a mass loss rate of $\dot{M} = 5\,\dot{M}_0$, in comparison to a model without mass loss. Therefore the direct influence of different mass loss rates on the nuclear evolution of WR stars can be neglected (cf. Schaerer 1996).

The dependence of the structure of the outer region of the star on the mass loss rate is very strong. E. g. the decrease of the photospheric luminosity relative to the nuclear luminosity, which is only about 20 % for the standard mass loss rate, becomes 94 % for five times that mass loss rate. This means that the nuclear luminosity $L_{\rm nuc}$ is 1.25 times larger than the stellar photon luminosity at infinity $L_\star$ in the first case, whereas it is 16 times larger in the second case.

To drive higher mass loss rates requires a higher rate of energy input into the wind, which may decrease the luminosity in the atmosphere of the star considerably. For a mass loss rate of about 5.44 $\dot{M}_0$, the energy which is required to drive the wind becomes so large that the luminosity at the photosphere vanishes and the photospheric temperature formally drops to 0. At this point the dashed line in Fig. 5 ends. Nevertheless, the inner Part of our models can be computed with higher mass loss rates to estimate that, even neglecting the kinetic energy of the wind, i. e. considering only the work against the gravitational potential, the mass loss rate could not exceed twice the limit given above. The energy budget in WR winds is discussed in the the following Section in more detail.

4. The luminosity of mass losing stars

Assuming stationarity, the flow of energy which is due to the wind flow is given by

$$L_{\rm W} = \dot{m}(r)\left(-\frac{Gm(r)}{r} + \frac{u^2}{2} + w\right) \tag{20}$$

(cf. Heger 1995), where $-\frac{Gm(r)}{r}$ is the gravitational potential, $\frac{u^2}{2}$ the specific kinetic energy, and w the specific enthalpy of the gas. For stationary models, the radial variation of the photon luminosity can then be written as

$$\frac{\mathrm{d}L}{\mathrm{d}r} = -\frac{\mathrm{d}L_{\rm W}}{\mathrm{d}r} + 4\pi r^2 \rho \epsilon_{\rm nuc} \quad . \tag{21}$$

The last term, which accounts for the nuclear energy production, is important in the core of the star (cf. central rise of L in Fig. 6), but can be neglected in the envelope and above.

In the hydrostatic region of the star, the work required to lift the matter in the star's gravitational field is almost balanced by the enthalpy gradient in these layers, and the kinetic energy does not contribute significantly. There, $L_{\rm W}$ remains small and the photon luminosity L decreases only slightly (see Fig. 6).

Above the sonic point, the potential energy term, and even more so the kinetic energy term in Eq. (20), become

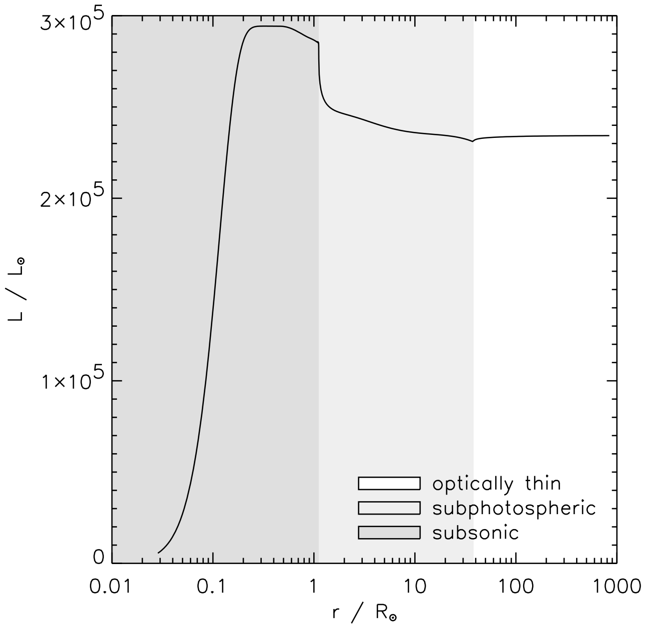

Fig. 6. Photon luminosity L as function of the radius r for our $15 \mathrm{M}_{\odot}$ standard model (cf. Section 2.4). The central increase is due to nuclear burning. The little dip at the photosphere (border between the light. grey and the white region) is artificial and results from the approximation in the derivation of Eq. (7) for the temperature stratification in a spherically extended atmosphere.

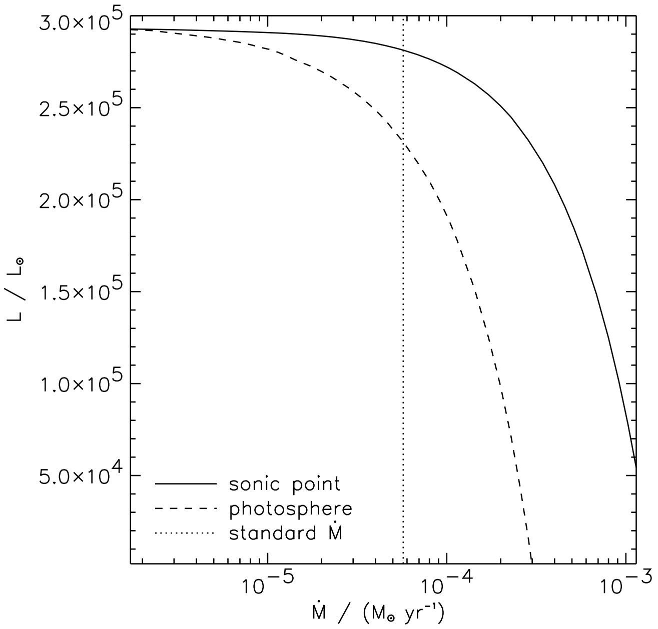

Fig. 7. Luminosity L at the sonic point (solid line) and at the photosphere (dashed line) for $15 \mathrm{M}_{\odot}$ models as function of the applied mass loss rate $\dot{M}$. Standard parameters have been used otherwise (cf. Section 2.4). The dotted line marks the standard mass loss rate $\dot{M}_0$.

large resulting in a significant decrease of the photon luminosity. For the standard model, it amounts to

$$\frac{\Delta L}{L_{\mathrm{nuc}}} \approx 0.2$$

(cf. Fig. 6), where the kinetic energy of the wind contributes as

$$\frac{\dot{M}_0 {u_\infty}^2}{2 L_{\mathrm{nuc}}} \approx 0.08 \quad .$$

Fig. 7 shows the photon luminosity at the sonic point (solid line) and at the photosphere (dashed line) as for various models with different mass loss rates. The luminosity at the sonic point and thus the stellar structure in the hydrostatic region is not affected much for mass loss rates as low as the standard mass loss rate. For higher values its influence becomes significant. In contrast, the photospheric luminosity is lowered for all values of $\dot{M}$.

Since the nuclear energy production of the star is almost independent of the mass loss rate (see Section 3.3), the radial decrease of the luminosity

$$\Delta L := L_{\mathrm{nuc}} - L_\star \tag{22}$$

does only depend on the mass loss rate $\dot{M}$ and the final velocity u_∞ of the wind. It is independent of the velocity law $u(r)$ of the wind.

We found that ΔL is well approximated by

$$\Delta L \approx \dot{M} \left(\xi \frac{GM}{R_{\mathrm{s}}} + \frac{{u_\infty}^2}{2} \right) \quad , \tag{23}$$

where the factor ξ corrects for the fact that the matter is not simply lifted from the hydrostatic radius of the star, but ultimately comes form layers deeper inside the star. We found that $\xi \approx 1.4$ is a good value for our standard model. In any case, the matter has to be lifted out of the potential at the hydrostatic radius, i. e. with negligible thermal contributions it is always $\xi \geq 1$. For WR star masses M in the range $5\mathrm{M}_{\odot} \leq M \leq 30\mathrm{M}_{\odot}$ (cf. Sect. 5.1), $\xi(M)$ is approximately given by the following fit:

$$\xi(M) = 1.8548 - 0.039711 \frac{M}{\mathrm{M}_{\odot}} + 6.1946\, 10^{-4} \left(\frac{M}{\mathrm{M}_{\odot}} \right)^2 \tag{24}$$

5. Mass-luminosity relation for WR stars

So far, there is not enough data available to gauge the mass-luminosity (M-L) relation for WR stars observationally, implying the particular need for an accurate theoretical relation. Maeder & Meynet (1987) found a linear relation in $\log L$ and $\log M$, while Langer (1989a), with more comprehensive calculations, obtained

$$\log \left(\frac{L_\star}{\mathrm{L}_{\odot}} \right) = a_0 + a_1 \log \left(\frac{M}{\mathrm{M}_{\odot}} \right) + a_2 \left(\log \left(\frac{M}{\mathrm{M}_{\odot}} \right) \right)^2 \tag{25}$$

(cf. also Schaerer & Maeder 1992, Beech & Mitalas 1992). The coefficients a_0, a_1 and a_2 are given in Table 2. However, hitherto the influence of mass loss on the luminosity $L_\star$ was neglected.

Table 2. Coefficients for the mass luminosity relations according to (25). The first line gives the coefficient found by Langer (1989a), the second line is our fit for the nuclear luminosity $L_{\rm nuc}$, and the third line gives the coefficients for the stellar photon luminosity $L_\star$. The last column gives the standard deviation.

	a_0	a_1	a_2	σ
Langer (1989)	2.357485	3.407930	−0.654431	
$L_{\rm nuc}$	2.507301	3.237961	−0.610150	0.003188
$L_\star$	2.107718	4.128283	−1.149148	0.011097

5.1. Wind darkening

To determine the effects of mass loss on the stellar luminosity, we calculate WR models for nine different masses in the range of 5 $M_\odot \dots 30$ $M_\odot$ with $\dot{M} = \dot{M}_0(M)$ (see Table 3). The other parameters of these models are the same as for the 15 $M_\odot$ standard model.

For comparison, we first derive a M-L relation from our models, neglecting the influence of the stellar wind, i. e. considering only $L_{\rm nuc}$ (cf. Eq. (17)); the result is show in Table 2 and Fig. 8. Slight differences of this relation with that of Langer (1989a) may be attributed to the differences in the opacities used for the model calculations.

A thoroughly different result is obtained for the stellar photon luminosity $L_\star$ (see Table 3) which is fitted by Eq. (25); the obtained coefficients are given in Table 2. Fig. 8 compares the nuclear and the photon M-L relations. The latter relation is shallower and lies below the nuclear M-L relation. For high masses, we find that the photon M-L relation is much lower than the nuclear M-L relation, whereas they agree better for lower masses. We designate the decrease of the photon luminosity due to the mass loss as *wind darkening* (cf. also Lucy & Abbott 1993).

Table 3. Nuclear luminosity $L_{\rm nuc}$ and observable luminosity $L_\star$ for different masses M, and their ratio.

$\frac{M}{M_\odot}$	$\log\left(\frac{L_{\rm nuc}}{L_\odot}\right)$	$\log\left(\frac{L_\star}{L_\odot}\right)$	$\frac{L_{\rm nuc}}{L_\star}$
5	4.47	4.44	1.08
6	4.66	4.62	1.09
8	4.94	4.89	1.11
10	5.14	5.08	1.14
12	5.29	5.22	1.17
15	5.47	5.37	1.26
20	5.68	5.55	1.36
25	5.84	5.64	1.57
30	5.96	5.68	1.91

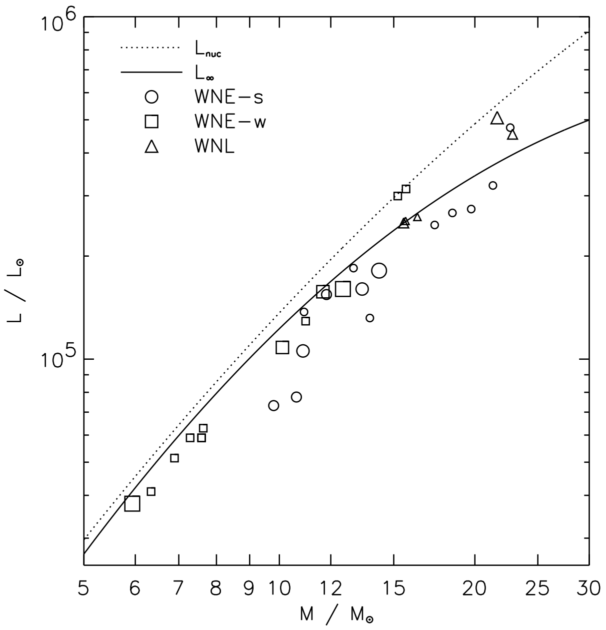

Fig. 8. Nuclear luminosity (dotted line) and the observable luminosity (solid line) for WR models with our standard mass loss rate, as a function of the stellar mass M (cf. Table 3). Also shown are the locations of 32 hydrogen-free WN stars considered by Hamann et al. (1995). Circles denote WNE-s stars, squares WNE-w stars and triangles WNL stars. The size of the symbols indicates the accuracy of the distance determination according to Hamann et al., with larger symbols indicating more reliable distances. The masses $M_{\rm new}$ shown in Table 4 are used here (see text).

Our results imply that the mass of a Wolf-Rayet star can not be derived from its observed luminosity only, but mass loss rate and terminal velocity of the wind need also to be taken into account. In particular, the wind darkening results in a larger derived mass for a given luminosity.

To obtain an impression of the importance of this effect, we calculate the masses of the 32 hydrogen-free WN stars analyzed by Hamann et al. (1995), using the values of $L_\star$, u_∞ and $\dot{M}$ given in their paper (which have been derived assuming a constant luminosity throughout the wind). With an iterative method, we compute complete stellar models to determine the mass $M_{\rm new}$ which a star has to have, so that its nuclear luminosity reduced by the luminosity necessary to drive the observed wind gives the observed luminosity. Therefore, we use Eq. (23) with $\xi(M)$ according to Eq. (24). The masses determined in this way are – as mentioned above – always larger than those obtained from the nuclear M-L relation; they are listed in Table 4 and illustrated in Figs. 8 and 9. Note that we do not compare our new M-L relation (Fig. 8) with empirical values from WR stars in binary systems (e. g. Howarth & Schmutz 1992) – which are explicitly left out in the sample of Hamann et al. (1995) – since internal mixing processes, which can act differently in single and binary stars, might lead to systematic deviations of the M-L relation for WR binary components from that for single stars (cf. Langer 1992).

Table 4. The 32 hydrogen-free WN stars analyzed by Hamann et al. (1995). In the first two columns, catalog number and WR spectral type are shown. In the third column, we give the masses $M_{\rm new}$ derived by including the wind darkening effect (see text), in the fourth column the difference $\Delta M = M_{\rm new} - M_{\rm old}$ between $M_{\rm new}$ and the masses $M_{\rm old}$ given in Hamann et al. (1995), and in the fifth column the relative change $\frac{\Delta M}{M_{\rm old}}$. Using $M_{\rm new}$, the nuclear luminosity $L_{\rm nuc}$ of the stars (column six) and their wind to photon momentum ratio η (last column) are determined according to Eqs. (25) and (26).

WR #	sp. type	$\frac{M_{\rm new}}{\rm M_\odot}$	$\frac{\Delta M}{\rm M_\odot}$	$\frac{\Delta M}{M_{\rm old}}$	$\log \frac{L_{\rm nuc}}{\rm L_\odot}$	$\frac{\dot M u_\infty}{L_{\rm nuc}/c}$
1	WNE-s	10.9	1.8	0.20	5.2	38.0
3	WNE-w	15.2	−0.1	−0.01	5.5	2.0
6	WNE-s	14.3	2.5	0.21	5.4	24.3
7	WNE-s	10.9	0.6	0.06	5.2	12.1
18	WNE-s	11.8	0.9	0.09	5.3	21.5
20	WNE-w	7.6	0.6	0.09	4.9	17.8
34	WNE-w	7.6	0.4	0.06	4.9	12.0
36	WNE-s	13.9	3.8	0.37	5.4	50.3
37	WNE-s	17.4	3.6	0.26	5.6	34.3
44	WNE-w	6.9	0.3	0.05	4.8	13.9
46	WNE-w	15.7	0.0	0.00	5.5	2.2
51	WNE-w	5.9	0.1	0.02	4.6	11.4
54	WNE-w	7.3	0.3	0.04	4.8	11.4
55	WNL	16.4	2.2	0.15	5.5	9.8
58	WNE-s	13.0	1.1	0.10	5.4	13.6
61	WNE-w	7.6	0.6	0.09	4.9	17.8
62	WNE-s	19.8	5.2	0.36	5.7	29.1
67	WNE-w	10.1	0.9	0.10	5.1	16.6
74	WNL	22.9	3.6	0.19	5.8	10.5
75	WNE-s	10.7	2.8	0.35	5.2	72.0
84	WNE-w	11.0	1.0	0.10	5.2	10.3
91	WNE-s	18.5	4.1	0.29	5.6	24.4
100	WNE-s	21.4	5.5	0.35	5.7	22.8
110	WNE-s	9.9	2.2	0.28	5.1	67.4
115	WNE-w	11.7	0.7	0.06	5.3	8.5
120	WNL	15.6	1.7	0.12	5.5	7.9
123	WNL	15.7	1.7	0.12	5.5	7.8
129	WNE-w	6.3	0.3	0.06	4.7	15.7
134	WNE-s	13.5	2.4	0.21	5.4	30.4
141	WNE-w	12.6	1.5	0.13	5.3	19.8
149	WNE-s	22.7	2.9	0.15	5.8	7.2
155	WNL	21.7	1.1	0.05	5.7	3.6

The new masses are found to be up to 37 % larger than previously estimated values. Even for low masses, where the nuclear and our improved M-L relation agree best, we find notable deviations. This means that the wind energy is not negligible even for small masses.

In Fig. 8, the observed WR stars are not located on a single M-L curve, but are scattered around the photon M-L relation obtained for models computed with our standard mass loss rate $\dot M_0$, and assuming $u_\infty = u_{\rm esc}(R_{\rm s})$ (cf. Section 2). This scatter is remarkable, since according to simple theoretical considerations all properties of H-free WN stars are expected to depend only on one single parameter, e. g. their mass (Langer 1989a). The most simple interpretation is that the scatter may be due to uncertainties in the values derived from observations ($L_\star$, $\dot M$ and u_∞). However, it is obvious from Fig. 8 (and also from Fig. 9 below) that stars of different WR spectral type deviate by different amounts from the M-L curve, with the strongest deviations found for the WNE-s stars. This implies either the presence of different systematic errors for $\dot M$- and $L_\star$-determinations for stars of different spectral types (cf. Howarth & Schmutz 1992, Schaerer 1996), or the presence of a second parameter affecting the structure of WR stars such that H-free WN stars of the same mass may have very different stellar winds.

Since the nuclear luminosity $L_{\rm nuc}$ depends on the mass with a power larger than 1, changes for this quantity due to the wind darkening correction are even larger than for the mass. This is relevant for the so called performance number

$$\eta := \frac{\dot M u_\infty}{L_{\rm nuc}/c} \quad , \tag{26}$$

which is the wind momentum flux in units of the photon momentum flux of the star. Especially for the stars with the highest performance numbers, i. e. many WNE-s stars, the value of η is decreased by more than a factor of 2 compared to the values listed in Hamann et al. (1995). E. g., for WR36 η reduces from 107 to 50 (cf. Table 4).

5.2. Mass – mass loss relation and maximum mass loss rate

For a given u_∞, there is a strict upper limit for the mass loss rate which a WR star may have due to energy considerations. To find its functional form, we calculate models for various stellar masses, at each mass increasing the mass loss rate until the photon luminosity at infinity vanishes. The limiting values $\dot M_{\rm max}$ found thereby are given in Table 5. They are well fitted by the linear relation

$$\dot M_{\rm max} = b_0 + b_1 \frac{M}{\rm M_\odot} \tag{27}$$

where

$b_0 = -1.03412\,10^{-4}\ {\rm M_\odot\ yr^{-1}}$ and

$b_1 = 2.76646\,10^{-5}\ {\rm M_\odot\ yr^{-1}}$.

Table 5. Standard mass loss rate $\dot{M}_0$ according to (16), maximum mass loss rate $\dot{M}_{\rm max}$, and their ratio.

$\frac{M}{{\rm M}_\odot}$	$\log\left(\frac{\dot{M}_0}{{\rm M}_\odot\ {\rm yr}^{-1}}\right)$	$\log\left(\frac{\dot{M}_{\rm max}}{{\rm M}_\odot\ {\rm yr}^{-1}}\right)$	$\frac{\dot{M}_{\rm max}}{\dot{M}_0}$
8	−4.95	−3.92	10.69
10	−4.70	−3.76	8.64
12	−4.50	−3.64	7.10
15	−4.24	−3.51	5.44
20	−3.92	−3.35	3.74
25	−3.67	−3.23	2.73

Fig. 9 shows that the standard mass loss rate approaches the maximum mass loss rate for high WR masses.

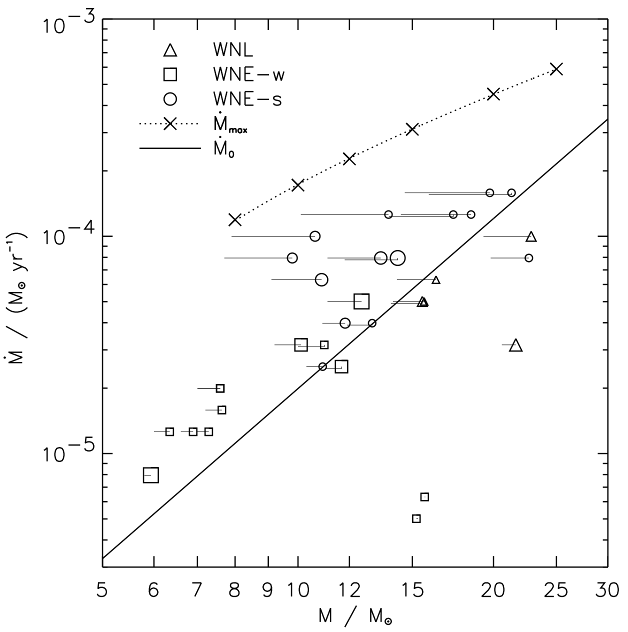

Fig. 9. Standard mass loss rate $\dot{M}_0$ (solid line) and maximum mass loss rate $\dot{M}_{\rm max}$ (dotted line) as function of the stellar mass M. The circles, squares and triangles have the same meaning as in Fig. 8. Thin horizontal lines adjoined to symbols illustrate the shift of the position of the stars in this diagram due to our new mass determinations. The center of the symbols marks their new positions, whereas the left end of each line shows their position according to Hamann et al. (1995).

Fig. 9 also shows the mass loss rates derived by Hamann et al. (1995) of the WN stars listed in Table 4, as function of their mass $M_{\rm new}$ (see Section 5.1 and Table 4). Despite of the larger new stellar masses, the observed mass loss rate are often still larger than the standard mass loss rate. Especially WNE-s stars show mass loss rates of a notable fraction of the maximum mass loss rate. We want to note here that, despite there are no stars observed with mass loss rates higher than the maximum mass loss rate, this would in principle be possible for winds with $u_\infty < u_{\rm esc}(R_{\rm s})$.

Furthermore, the mass corrections introduced in Section 5.1, which are indicated by the thin horizontal lines in Fig. 9, considerably reduce the scatter of the empirical $\dot{M}$ vs. M data points. However, as in Fig. 8, in particular the WNE-s stars continue to form a subgroup distinctly different from the other spectral types. The question whether or not this indicates just different systematic errors (cf. Howarth & Schmutz 1992, Schaerer 1996), or points towards two different classes of H-free WN stars needs to be answered by future studies of these objects.

6. Conclusions

We have calculated stationary models of WR stars by solving the hydrodynamic stellar structure equations up to a supersonic boundary velocity, including a grey, optically thick wind. These models allow the investigation of the influence of an optically thick wind on the internal structure of WR stars as well as on the layers in the vicinity of the sonic point. This method, together with appropriate outer boundary conditions, allows also an analysis of the radial dependence of the energy budget in the stellar wind, and in particular a determination of the stellar photon luminosity at infinity, $L_\star$. The obtained results can be summarized as follows.

- The structure of the deep internal layers of WR stars are practically not affected by the presence of a strong wind. In particular, the local rates of nuclear energy production, the central values of T and ρ, and the size of the convective core remain constant (cf. also Schaerer 1996)
- The radius of the sonic point of the wind flow, for a WR star of given mass, changes only by a few percent, even when the wind parameters are changed by orders of magnitude. Moreover, it is almost identical to the radius of a helium star of the same mass but without mass loss. Correspondingly small radii are confirmed by recent studies of very close WR+O binary systems (Moffat & Marchenko 1996).
- Certain wind parameters result in the fact that the iron opacity peak basically coincides with the sonic point. We speculate about self-regulating mechanisms which naturally provide just the wind parameters required for this condition, which may be related with the large observed WR mass loss rates (cf. also Pistinner & Eichler 1995).
- The observable photon luminosity of a WR star may be considerably smaller than the luminosity generated by nuclear burning in the deep interior. This *wind darkening* is found to essentially depend on the mass loss rate, the final wind velocity, and the sonic point radius.

- Taking wind darkening into account considerably reduces the scatter in the $\dot{M}$ vs. M diagram of H-free WN stars (Fig. 9). It furthermore reduces the so called momentum problem of WR winds by up to a factor of two.
- If the stellar wind parameters depend only on the stellar mass, H-free WN stars can still be expected to obey a unique mass-luminosity relation. However, the wind darkening should be taken into account, since its neglect leads to a severe underestimate of the mass of a WR star when derived from its photon luminosity (cf. Fig. 8).
- In case the wind properties of H-free WN stars depend on more then one parameter, they would not obey a unique mass-luminosity relation due to the effect of wind darkening. Such a scenario may be indicated by the distinct separation of the WNE-s stars from other H-free WN stars in the M-L and $\dot{M}$-M-diagram (Figs. 8 and 9).

Acknowledgements. We are grateful to Hartmut Braun, Jens Fliegner, Wolfgang Hillebrandt, Peter Höflich, Henny Lamers, Leon Lucy, Stan Owocki, Daniel Schaerer and Uwe Springmann for illuminating discussions. This work has been supported by the Deutsche Forschungsgemeinschaft through grants La 587/8-1,2.

References

Beech M., Mitalas R., 1992, A&A 262, 483
Chiosi C., Maeder A., 1986, ARA&A 24, 329
Eichler D., Bar Shalom A., Oreg J., 1995, ApJ 448, 858
Glatzel W., Kiriakidis M., Fricke K.J., 1993, MNRAS 262, L7
Hamann W.-R., 1995, in: Wolf-Rayet Stars: Binaries, Colliding Winds, Evolution, eds. K. A. Van der Hucht, P. M. Williams, IAU Symp. 163 Kluwer, Dordrecht, p. 105
Hamann W.-R., Koesterke L., Wessolowski U., 1995, A&A 299, 151
Heger A., 1995, Diploma thesis, TU München
Henyey L.G., Forbes J.E., Gould N.L., 1964, ApJ 139, 306
Hillier D.J., 1995, in: Wolf-Rayet Stars: Binaries, Colliding Winds, Evolution, eds. K. A. Van der Hucht, P. M. Williams, IAU Symp. 163 Kluwer, Dordrecht, p. 116
Hofmeister E., Kippenhahn R., Weigert A., 1964, Zeitschrift für Astrophysik 59, 215
Howarth I.D., Schmutz W., 1992, A&A 261, 503
Huebner W.F., Merts A.L., Magee N.H., Argo M.F. Jr., 1977, Astrophys. Opacity Library, LA-6760-M
Iglesias C.A., Rogers F.J., Wilson, B.G., 1992, ApJ 397, 717
Kippenhahn R., Weigert A., 1991, Stellar Structure and Evolution, Springer-Verlag, Berlin
Kiriakidis M., 1993, PhD Thesis, Göttingen
Kudritzki R.-P., 1988, in: Radiation in Moving Gaseous Media, eds. Chmielewski Y., Lanz T., Geneva Observatory, Sauverny-Versoix, p. 1
Lamers H.J.G.L.M., Maeder A., Schmutz W., Cassinelli J.P., 1991 ApJ 368, 538
Langer N., 1989a, A&A 210, 93
Langer N., 1989b, A&A 220, 135
Langer N., 1992, A&A 265, L17
Lucy L. B., 1971, ApJ 163, 95
Lucy L. B., 1976, ApJ 205, 482
Lucy L. B., Abbott, D. C., 1993, ApJ 405, 738
Maeder A., Conti P.S., 1994, ARA&A 32, 227
Maeder A., Meynet G., 1987, A&A 182, 243
Moffat A.F.J., Marchenko S.V., 1996, A&A 305, L29
Morris P.W., 1995, in: Wolf-Rayet Stars: Binaries, Colliding Winds, Evolution, eds. K. A. Van der Hucht, P. M. Williams, IAU Symp. 163 Kluwer, Dordrecht, p. 96
Owocki S.P., Gayley K.G., 1995, in: Wolf-Rayet Stars: Binaries, Colliding Winds, Evolution, eds. K. A. Van der Hucht, P. M. Williams, IAU Symp. 163 Kluwer, Dordrecht, p. 138
Pistinner S., Eichler D., 1995, ApJ 454, 404
Schaerer D., 1996, A&A 309, 129
Schaerer D., Maeder, A., 1992, A&A 263, 129
Schmutz W., 1995a, in: Wolf-Rayet Stars: Binaries, Colliding Winds, Evolution, eds. K. A. Van der Hucht, P. M. Williams, IAU Symp. 163 Kluwer, Dordrecht, p. 127
Schmutz W., 1995b, submitted
Springmann U., 1994, A&A 289, 505

This article was processed by the author using Springer-Verlag LaTeX A&A style file *L-AA* version 3.